PHOTONICS Research

Single-sideband microwave-to-optical conversion in high-Q ferrimagnetic microspheres

Cheng-Zhe Chai,[1,2,†] Zhen Shen,[1,2,†] Yan-Lei Zhang,[1,2] Hao-Qi Zhao,[1,2,3] Guang-Can Guo,[1,2] Chang-Ling Zou,[1,2] and Chun-Hua Dong[1,2,*]

[1]CAS Key Laboratory of Quantum Information, University of Science and Technology of China, Hefei 230026, China
[2]CAS Center for Excellence in Quantum Information and Quantum Physics, University of Science and Technology of China, Hefei 230026, China
[3]Current address: Department of Electrical and Systems Engineering, University of Pennsylvania, Philadelphia, Pennsylvania 19104, USA
*Corresponding author: chunhua@ustc.edu.cn

Received 20 October 2021; revised 23 January 2022; accepted 24 January 2022; posted 25 January 2022 (Doc. ID 446226); published 1 March 2022

Coherent conversion of microwave and optical photons can significantly expand the capabilities of information processing and communications systems. Here, we experimentally demonstrate the microwave-to-optical frequency conversion in a magneto-optical whispering gallery mode microcavity. By applying a magnetic field parallel to the microsphere equator, the intracavity optical field will be modulated when the magnon is excited by the microwave drive, leading to a microwave-to-optical conversion via the magnetic Stokes and anti-Stokes scattering processes. The observed single-sideband conversion phenomenon indicates a nontrivial optical photon–magnon interaction mechanism derived from the magnon that induced both the frequency shift and modulated coupling rate of optical modes. In addition, we demonstrate the single-sideband frequency conversion with an ultrawide tuning range up to 2.5 GHz, showing its great potential in microwave-to-optical conversion.

https://doi.org/10.1364/PRJ.446226

1. INTRODUCTION

Electromagnetic waves at microwave and optical frequencies play important roles in information processing and communications systems. However, the quantum information technology based on the most promising superconducting qubits is operated at cryogenic temperature with microwave photons, which cannot achieve long-distance communications between qubits. Unlike microwave photons, the optical photon can transmit via low loss optical fibers, making them suitable for long-distance communications. Thus, frequency conversion between a microwave photon and an optical photon has attracted great interest [1–6]. Besides, the energy of a single microwave photon is too low to be efficiently detected with a high signal-to-noise ratio (SNR). In contrast, converting the microwave photons to optical photons can be detected directly with single-photon detectors. Therefore, it can greatly promote the detection based on the microwave, help to improve the resolution of radar, and maybe realize the quantum-enhanced radar system [7]. Recently, such a microwave-to-optical transducer [6] has been demonstrated in optomechanics, electro-optic interaction, atoms, and ions [8–17]. Among these approaches, optomagnonics based on a magnon provides an alternative and attractive approach to the coherent microwave-to-optical conversion because of its great frequency tuning range and long coherence time [18–24]. Besides, due to the nonlinearity of the system, high-order sidebands can be generated in optomagnonics [25].

Currently, frequency conversion has been demonstrated in such an optomagnonic system [26–30], where the high-Q yttrium iron garnet (YIG) whispering gallery mode (WGM) microcavity was used to enhance the interaction between magnons and photons, and nonreciprocity of the magnetic Brillouin light scattering (BLS) has been observed [28,31]. However, similar to the Brillouin optomechanical system [32,33], the triple-resonance condition (the phase matching between pump, signal, and magnetic modes) is required in such systems, which may limit the flexibility in choosing the working frequencies and tunability of the frequencies. Therefore, using the great tunability of the magnon and also the two-mode magnon–photon coupling mechanism would allow us to achieve the transducer that mitigates the limitations mentioned above.

In this paper, a tunable frequency conversion between microwave and photons is realized by the dynamical Faraday effect in a YIG microsphere. The magnetic Stokes and anti-Stokes scattering induced by the dispersive interaction between the magnon mode and the optical mode can be observed.

When the frequency of the pump light is resonant with the optical mode, the asymmetry of the two sidebands and even a single sideband (SSB) is observed in our experiment. By changing the direction of the static external magnetic field, we observed both the optical mode resonance frequency shift and the modulated coupling efficiency, corresponding to both phase and intensity modulations. Therefore, we deduced that this asymmetry conversion is derived from the phase and intensity modulations induced by the internal magnetization procession. In our experiment, we demonstrated 16 times asymmetry of the two sidebands and a magnon tuning range of 2.5 GHz, corresponding to the tunable frequency conversion with the same range. We believe, to the best of our knowledge, that our results serve as a novel method for the implementation of SSB microwave-to-optical conversion devices.

2. EXPERIMENTAL SETUP AND RESULTS

The principle of the frequency conversion in the YIG microsphere is illustrated in Fig. 1(a). The input light couples to the YIG microcavity and excites the WGMs through the high-index prism. The WGMs in the microcavity will have a spin along the z direction due to the spin-orbit coupling of light [34–36]. According to our previous work, the spin will be modulated by the magnetization along the z direction due to the Faraday effect, thus shifting the resonant frequency of the WGMs [34]. When applying a magnetic field parallel to the resonator equator, the microwave excites the magnon mode in the microcavity by an antenna and causes the procession of the magnetization in the microcavity. Therefore, as shown in Fig. 1(c), the resonant frequency of the optical mode in the microcavity will be modulated by the magnetization

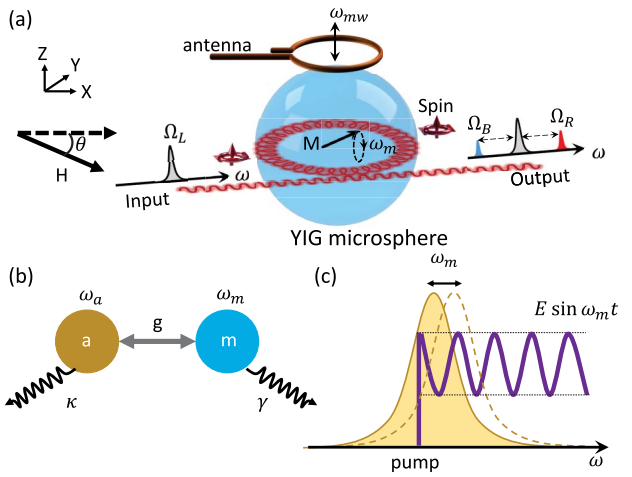

Fig. 1. (a) Schematic of the microwave-to-optical frequency conversion in a YIG microsphere. The bias magnetic field is parallel to the optical path, while the input light excites the WGMs and has an optical spin perpendicular to the propagating direction due to the spin-orbit coupling. The intracavity field could be modulated by the dynamic magnetic field via the Faraday effect, and generate two sidebands at the output port. (b) Frequency conversion via the coupling between photon (a) and magnon (m). (c) Illustration of the dispersive magnon–photon coupling as the magnetization-induced modulation of the resonant frequency.

procession. When an optical pump drives at the optical mode, its amplitude will be modulated and lead to two sidebands at the output as an oscillator system, and the Hamiltonian of the system can be written as

$$H = \omega_a a^\dagger a + \omega_m m^\dagger m + g a^\dagger a (m + m^\dagger), \tag{1}$$

where $a(a^\dagger)$ and $m(m^\dagger)$ are the annihilation (creation) operators for optical mode and magnon mode, respectively. g is the magneto-optical coupling strength, and ω_a and ω_m are the frequency of the optical mode and magnon mode, respectively. Different from the previous experiment based on a triple-resonance condition [26–29], only one optical mode and one magnon mode participated in the magneto-optical interaction, as shown in Fig. 1(b). Therefore, the interaction between the photon and the magnon in our experiment is similar to the two-mode interaction in an optomechanical system [37]. Considering the great tunability of the magnon, a larger operating frequency transducer could be obtained than what has been reported in previous optomagnonic system research.

Figure 2(a) is the schematic of our experimental setup. A tunable diode laser is separated into two laser beams by an optical fiber splitter. One beam excites the WGMs by the rutile prism, and would generate two sidebands due to the interaction between the magnons and photons. Another laser beam is shifted with a frequency of +80 MHz by an acousto-optical

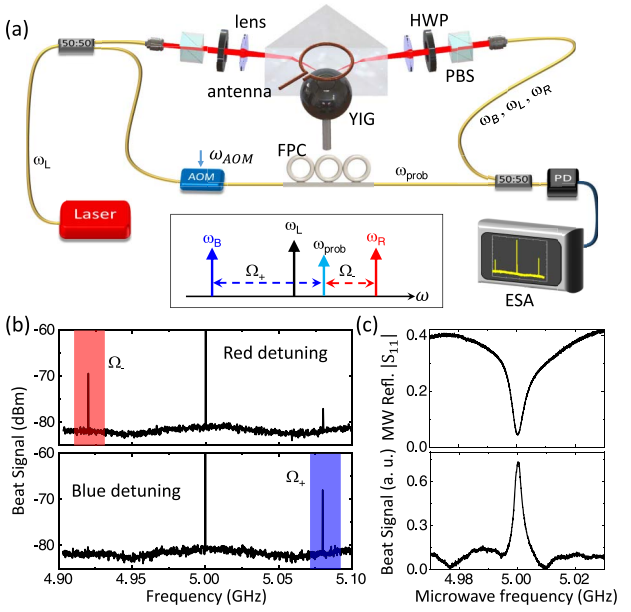

Fig. 2. (a) Schematic of the experimental setup. A tunable laser is separated into two beams by an optical fiber splitter. One beam excites the WGMs by prism coupling, which would generate two sidebands at the output, and then combines another beam as the local oscillator (LO) is shifted by an acousto-optical modulator (AOM). PBS, polarization beam splitter; HWP, half-wave plate; FPC, fiber polarization controller; PD, photon detector; ESA, electric spectrum analyzer. Inset: spectral position of the pump laser, the sidebands, and the probe laser as the local oscillator. (b) The detected beat signal when the optical pump is at red and blue detunings, respectively. The $\Omega_-(\Omega_+)$ corresponds to the sideband signal, which is higher (or lower) than the optical pump. (c) Microwave reflection and the generated beat signal as a function of the microwave frequency.

modulator (AOM) as the local oscillator (LO) to measure the sidebands through heterodyne measurement, as shown in the inset of Fig. 2(a). Two laser beams are combined with the beam splitter and sent to a 12 GHz high-speed photon detector followed by a microwave amplifier and a spectrum analyzer. In our experiment, the radius of the YIG microsphere is about 400 μm. Two sets of polarization beam splitters and half-wave plates are used to control the polarization of the system. One is to excite the different polarized WGMs, and the other is to verify the polarization of the generated sideband signal, which is consistent with the pump light. A fiber polarization controller is used to make two light paths have the same polarization to optimize the beat signal. The magnon mode used in the experiment is the uniform mode known as the Kittel mode, whose frequency is determined by $\omega_m = \gamma H$, where $\gamma = 2\pi \times 2.8$ MHz/Oe is the gyromagnetic ratio and H is the external bias magnetic field. The external static magnetic field with an intensity of approximately 1780 Oe is parallel to the resonator equator, corresponding to the magnon frequency of approximately 5 GHz, and the Kittel mode is excited by an antenna placed above the YIG microsphere, with the microwave power amplified up to about 500 mW.

The pump laser with a frequency of ω_L modulated by the dynamic Faraday effect through the YIG microcavity will be scattered to two sidebands (ω_R and ω_B). The LO beam has a +80 MHz frequency shift with respect to the pump laser. As a result, the sideband signal ω_R (or ω_B) is measured through the beat signals Ω_- (or Ω_+) in the spectrum analyzer, as shown in Fig. 2(b). The typical results are measured when the optical pump has a red (or blue) detuning from the optical mode set equal to the magnon frequency, which indicates the anti-Stokes (or Stokes) scattering. Figure 2(c) shows the microwave reflection and the generated beat signal (Ω_-) as a function of the microwave frequency via a vector network analyzer (VNA). The beat signal shows a resonant characteristic and correlates to the magnon mode, which verified the participation of the magnon in the frequency conversion process.

When the pump laser is scanning through the cavity modes, the typical transmission is shown in Fig. 3(a). The dotted line is a Lorentz fitting, corresponding to the loaded Q factor of 4.7×10^5. Figure 3(b) shows the converted signals (Ω_- or Ω_+) obtained with the same optical mode by scanning the pump laser. When the pump laser is red detuning with a magnon frequency, the sideband ω_R is resonant with the optical mode and another sideband ω_B is far detuned, thus generating the fairly strong sideband ω_R in the optical spectrum, the anti-Stokes scattering dominant at this situation. Therefore, the signal of Ω_- is only observed. On the contrary, the signal of Ω_+ is only observed when the pump laser is blue detuning. In particular, when the pump laser is resonant with the optical mode, the modulation of the optical resonant would induce two sidebands, as obviously shown by both the signals of Ω_- and Ω_+. Therefore, the signal of Ω_- and Ω_+ has a similar shape, just with a magnon frequency shift.

Surprisingly, when the pump laser is resonant with the optical mode, the two sidebands signals are asymmetric in Fig. 3(b), in contrast to the symmetric sidebands reported in the dispersively coupled optomechanical systems [38,39].

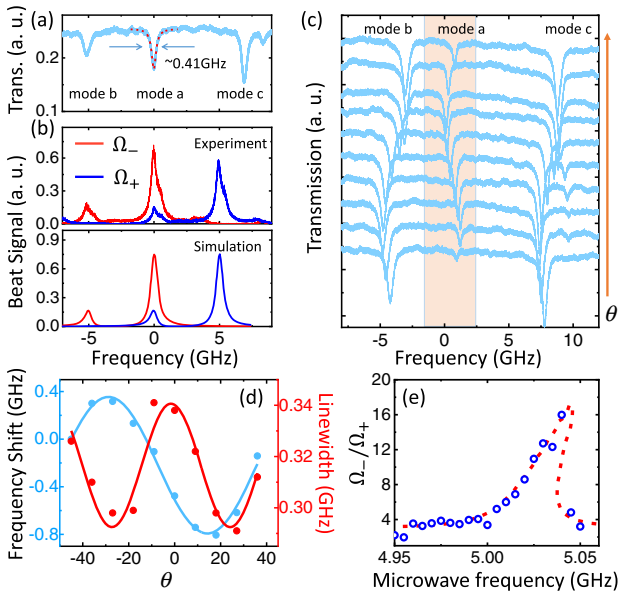

Fig. 3. (a), (b) Optical pump transmission and the generated optical signal as a function of the pump laser frequency. The experimental results agree well with the numerical calculations. (c) Transmission as a function of the input light frequency with different bias magnetic field direction. (d) The frequency shift and linewidth of the optical mode as a function of the bias magnetic field direction from (c). (e) Ω_-/Ω_+ ratio as a function of the input microwave frequency. The red dotted line represents the fitting result when considering the thermal effect of magnon.

To investigate the physical mechanism for this novel SSB phenomenon, Fig. 3(c) shows the optical transmission when changing the magnetic field direction, corresponding to the magnetic field direction changed with the microwave signal. The angle θ between the magnetic field direction and the resonator equator is changed from −45° to 40°. The transmission of the target optical mode for the efficient frequency conversion has an obvious change during the adjustment, as shown in the gray region of Fig. 3(c), while the transmission of other optical modes has no obvious change during the process. These results indicate that the changed magnetization direction of the YIG sphere could significantly change the coupling strength of the target resonance mode with a near-field coupler. Figure 3(d) further shows the resonant frequency and linewidth as a function of the θ. It indicates that both the resonant frequency and linewidth of the optical mode could also be modulated by the dynamic magnetic field and the two modulations have a phase difference $\sim\pi$, corresponding to the novel magnon-photon coupling that induces out-of-phase dispersive and dissipative modulations. Similar to the optical SSB modulator [40], such out-of-phase phase modulation (frequency) and intensity modulation (coupling strength) eventually lead to the SSB microwave-to-optical conversion.

To consider the optical mode owning two modulations with the dynamic magnetic field induced by the microwave, one is the frequency modulation $ga^\dagger a(m + m^\dagger)$ shown in Eq. (1), and the other one is the coupling strength modulation, where $\kappa_{a,1}$ could be expressed as $\kappa_{a,1}[1 + A(m + m^\dagger)]$, and

where A is the modulation coefficient of the coupling strength. The coupled-oscillator equations in the interaction picture are then rewritten as

$$\frac{\mathrm{d}a}{\mathrm{d}t} = \left(i\Delta_a - \frac{\kappa_a}{2}\right)a - iga(me^{-i\omega_{\mathrm{mw}}t} + \mathrm{H.c.}) + \sqrt{\kappa_{a,1}}[1 + A(me^{-i\omega_{\mathrm{mw}}t} + \mathrm{H.c.})/2]\sqrt{\frac{P_L}{\hbar\omega_L}}, \quad (2)$$

$$\frac{\mathrm{d}m}{\mathrm{d}t} = \left(i\Delta_m - \frac{\kappa_m}{2}\right)m - iga^{\dagger}ae^{i\omega_{\mathrm{mw}}t} + \sqrt{\kappa_{m,1}}\sqrt{\frac{P_{\mathrm{mw}}}{\hbar\omega_{\mathrm{mw}}}} + \left(A\sqrt{\kappa_{a,1}}/2\right)\sqrt{\frac{P_L}{\hbar\omega_L}}(a - a^{\dagger})e^{i\omega_{\mathrm{mw}}t}, \quad (3)$$

where $\Delta_a = \omega_L - \omega_a$ and $\Delta_m = \omega_{\mathrm{mw}} - \omega_m$ are the detuning of the optical and the microwave pump, respectively. κ_a (κ_m) is the decay rate of the optical (magnon) mode. The numerical results are shown in Fig. 3(b). In Fig. 3(b), one can see that the experimental and numerical results are in good agreement, which further verifies the two modulations on the optical mode that causes the SSB phenomenon. Further studies have found that when the pumped laser is kept at the near-resonance position, the ratio of the beat frequency signal between the red and blue (Ω_-/Ω_+) sidebands changes with different microwave detuning. The magnon frequency is 5 GHz and it is found that the ratio of the beat frequency signal has distinct resonant properties, which means the stronger driving force of microwave enhances the precession amplitude of the magnon along the z axis near the resonator equator, leading to the stronger SSB effect, as shown in Fig. 3(e). The resonant frequency in Fig. 3(e) is larger than 5 GHz because of the thermal effect on the magnon [41].

As we know, the external magnetic field can tune the frequency of the magnon, corresponding to the tunable frequency conversion. Figure 4 shows the frequency conversion when only tuning the relevant magnon frequency from 3.5 to 6 GHz, a range that is limited by the permanent magnet we used. It shows that our device has a much larger operation bandwidth compared to the previous scheme [26–29]. Taking the insertion losses into consideration, the power conversion efficiency in our experiment is estimated as 3.62×10^{-6}, corresponding to the photon number conversion efficiency of 0.94×10^{-10}. Despite the fact that the conversion efficiency is lower than that of the previous experiment based on a triple-resonance condition [26–30], our experiment provides a novel method to realize the SSB frequency conversion between microwave and optical photons.

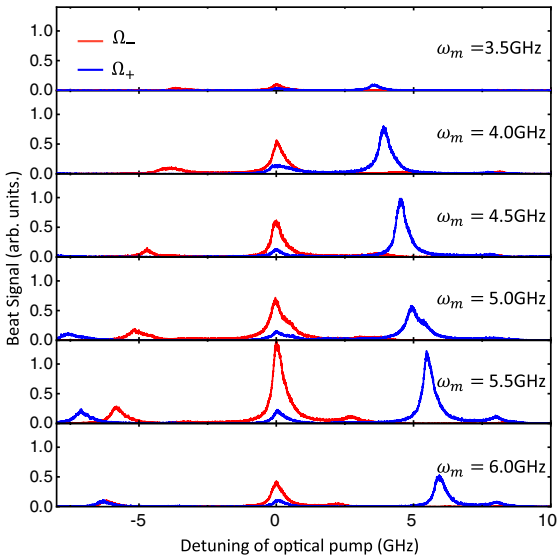

Fig. 4. Converted signal as a function of the pump laser frequency detuning with different magnon frequencies by changing the magnetic field.

The conversion efficiency can be improved by introducing a second microcavity to approach the first microcavity, so that the optical mode will split due to strong coupling between two microcavities [10]. The coupling strength is tunable, so the splitting of the optical mode can be selected to match the required magnon frequency to achieve the optical pump and sideband signal resonant with the optical modes. Then the photon number conversion efficiency $\eta \propto \frac{\kappa_{m,1}\kappa_{a,1}}{\kappa_m\kappa_a}\frac{4C}{(1+C)^2+(\Delta/\kappa_a)^2}$ with $C = \frac{4g^2\langle a^{\dagger}a\rangle}{\kappa_m\kappa_a}$ could be increased by 70 times when Δ is changed from ω_m to 0. In addition, scaling down the size of the YIG microsphere to reduce the mode volume, or replacing the microsphere with a microdisk and using a high-order magnetic mode to improve the mode overlap [28,30,42,43], the coupling strength $g/2\pi$ could be increased by a factor of about 100, leading to a frequency conversion efficiency of four orders of magnitude larger. Finally, polishing the YIG microsphere and using a high-index waveguide can reduce κ_a and improve the $\kappa_{a,1}$, and η can be increased by about 20 times. With these improvements, the predicted photon number conversion efficiency can be improved to about 1.3×10^{-3}.

3. CONCLUSION

We experimentally demonstrate the SSB frequency conversion between microwave and optical photons in a YIG microcavity. By applying the static magnetic field parallel to the resonator equator, the magnetic Stokes and anti-Stokes scattering occurs in the YIG microsphere, which resembles the phonon–photon interaction in an optomechanical system. Besides, due to the modulation of both the resonance frequency and external coupling intensity of optical modes, the SSB modulation has been demonstrated in our experiment. Our results provide what we believe is a novel method to realize the SSB frequency transducer.

APPENDIX A

The optical transmissions measured in our experiment are shown in Fig. 5. The refractive index of the a YIG microsphere at a 1550 nm wavelength is 2.19; thus, we chose the rutile coupling prism (ADT-6, Thorlabs) to get better mode match. As shown in Fig. 5, the high-Q optical modes can be found in both TE and TM spectra. The TE and TM modes have a free spectral range of about 54.1 GHz and 54.9 GHz, respectively, which correspond to the radius of the YIG microsphere (about 400 μm) used in our experiment. The transmission of TE and TM modes is different due to the birefringence of the rutile

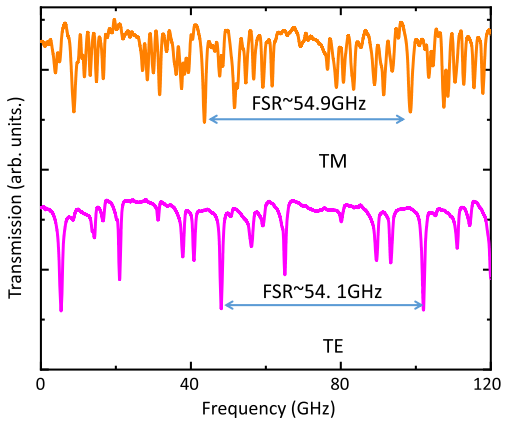

Fig. 5. Typical transmission of the YIG microcavity with TE and TM modes via prism coupling.

coupling prism, which has the optic axis perpendicular to the equatorial plane of the YIG microsphere. For the same incident direction of laser into the prism, the TE mode and the TM mode will have a different refractive index, leading to different wave vectors of the evanescent field. Considering the phase matching in prism coupling, the different incident evanescent field will lead to different measured transmissions. It should be pointed out that when changing the polarization from TE to TM modes in our experiment, the YIG microsphere must slightly move in the equatorial plane direction to achieve the best coupling efficiency.

APPENDIX B

In our research, we also found that the strength of the magnetic field will affect the transmission. As shown in Fig. 6, the direction of the magnetic field is parallel to the equatorial plane of the YIG microsphere, and the transmission is measured when changing the magnetic strength zero to saturation. Note that the saturation magnetic field of the YIG is 1780 Oe. It is obvious that the linewidth and resonance frequency of the optical mode in the blue area change with the magnetic field strength, but the two other optical modes are hardly changed.

To verify that the single-sideband effect we observed is not caused by an accidental optical mode, we determined that the transmission at the magnetic strength is zero and saturation in a free optical spectral region (FSR), as shown in Fig. 7. Multiple optical modes can be found in the free spectral region, and their coupling efficiency is significantly modulated by the strength of the magnetic field. Therefore, by measuring the relationship between the sideband signal and the pump light detuning around these optical modes, one can clearly observe the single-sideband effect, which verifies the conclusion in our main text.

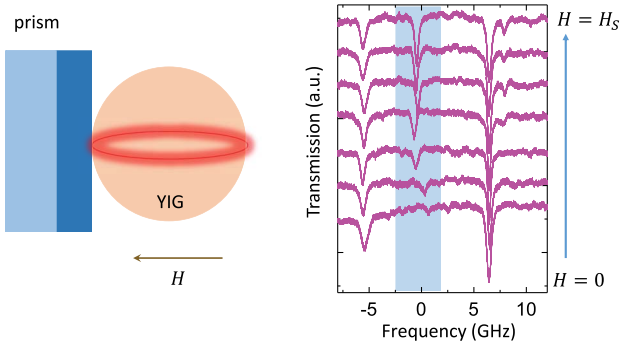

Fig. 6. Transmission as a function of the input light frequency with different bias magnetic field strength.

APPENDIX C

In our experiment, there is only one optical mode and one magnon mode that participate in the magneto–optical interaction. As mentioned in the main text, the Hamiltonian of the system is

$$H = \omega_a a^\dagger a + \omega_m m^\dagger m + g a^\dagger a (m + m^\dagger), \tag{C1}$$

where $a(a^\dagger)$ and $m(m^\dagger)$ are the annihilation (creation) operators for the optical pump mode and magnon mode, respectively. g is the coherent magneto-optical coupling strength and can be expressed as

$$g = \frac{\varepsilon_0}{2} i f \eta \int (u_r^* u_\phi - u_r u_\phi^*) \mathrm{d}\mathbf{x}^3, \tag{C2}$$

where u_x is the x component of normalized electrical field $\overleftarrow{u}(\mathbf{x})$ with $x \in \{r, \phi, z\}$, ε_0 is the vacuum permittivities of the material, and $f = \frac{2\sqrt{\varepsilon_r}\phi_r}{k_0 M_0}$ is the coefficient of the magneto–optical effect in which ε_r, ϕ_r, k_0, and M_0 are, respectively, the relative permittivity, Faraday rotation, wave number, and the saturation magnetization of the YIG. $\eta = \frac{g_s \mu_B \sqrt{2sN}}{2V}$, where $g_s = 2$ is Lande g factor, μ_B is Bohr magneton, $N = \rho V$ is the total spin population of the sphere, $\rho = 4.22 \times 10^{27} \mathrm{m}^{-3}$ is the spin density, $s = \frac{5}{2}$ is the spin number of YIG, and V is the volume of sphere. The integral term in Eq. (C2) represents the chirality of light.

Under external optical and microwave drive, the Hamiltonian of the system is

$$\begin{aligned} H = {} & \omega_a a^\dagger a + \omega_m m^\dagger m + g a^\dagger a (m + m^\dagger) \\ & + \sqrt{\kappa_{m,1}} \sqrt{\frac{P_{\mathrm{mw}}}{\hbar \omega_{\mathrm{mw}}}} (m^\dagger e^{-i\omega_{\mathrm{mw}} t} - m e^{i\omega_{\mathrm{mw}} t}) \\ & + \sqrt{\kappa_{a,1}} \sqrt{\frac{P_L}{\hbar \omega_L}} (a^\dagger e^{-i\omega_L t} - a e^{i\omega_L t}). \end{aligned} \tag{C3}$$

Here, ω_L and P_L are the frequency and power of input pump laser, ω_{mw} and P_{mw} are that of the microwave signal input, and $\kappa_{m,1}$ and $\kappa_{a,1}$ are the external coupling rate for the two modes, respectively. As mentioned in the main text, the optical mode has two modulations: the frequency modulation $g a^\dagger a (m + m^\dagger)$, and the coupling strength $\kappa_{a,1}$ which has a modulation expressed as $\kappa_{a,1}[1 + A(m + m^\dagger)]$ [44], where A is a constant. Then, the equations of motion in the rotating frame can be written as

Table 1. Parameters Used in the Numerical Simulations

Parameter	Symbol	Value
External coupling rate of the optical mode	$\kappa_{a,1}$	$2\pi \times 0.03$ GHz
Decay rate of the optical mode	κ_a	$2\pi \times 0.6$ GHz
External coupling rate of the magnon mode	$\kappa_{m,1}$	$2\pi \times 3$ MHz
Decay rate of the magnon mode	κ_m	$2\pi \times 8.6$ MHz
Optical pump power	P_L	0.01 W
Microwave pump power	P_{mw}	1 W
Frequency of the optical mode	ω_L	$2\pi \times 193$ THz
Frequency of the magnon mode	ω_m	$2\pi \times 5$ GHz
Modulation constant of $\kappa_{a,1}$	A	1
Coupling strength of the magneto–optical interaction	g	$2\pi \times 6$ Hz

$$\frac{\mathrm{d}a}{\mathrm{d}t} = \left(i\Delta_1 - \frac{\kappa_a}{2}\right)a - iga(me^{-i\omega_{\mathrm{mw}}t} + \mathrm{H.c.}) + \sqrt{\kappa_{a,1}}[1 + A(me^{-i\omega_{\mathrm{mw}}t} + \mathrm{H.c.})/2]\sqrt{\frac{P_L}{\hbar\omega_L}}, \tag{C4}$$

$$\frac{\mathrm{d}m}{\mathrm{d}t} = \left(i\Delta_2 - \frac{\kappa_m}{2}\right)m - iga^{\dagger}ae^{i\omega_{\mathrm{mw}}t} + \sqrt{\kappa_{m,1}}\sqrt{\frac{P_{\mathrm{mw}}}{\hbar\omega_{\mathrm{mw}}}} + (A\sqrt{\kappa_{a,1}}/2)\sqrt{\frac{P_L}{\hbar\omega_L}}(a^{\dagger} - a)e^{i\omega_{\mathrm{mw}}t}, \tag{C5}$$

where we have assumed $\sqrt{1 + A(me^{-i\omega_{\mathrm{mw}}t} + \mathrm{H.c.})} \approx 1 + A(me^{-i\omega_{\mathrm{mw}}t} + \mathrm{H.c.})/2$ for $A(me^{-i\omega_{\mathrm{mw}}t} + \mathrm{H.c.}) \ll 1$. κ_a (κ_m) is the decay rate of the optical (magnon) mode, and $\kappa_a = \kappa_{a,0} + \kappa_{a,1}[1 + A(me^{-i\omega_{\mathrm{mw}}t} + \mathrm{H.c.})]$ ($\kappa_m = \kappa_{m,0} + \kappa_{m,1}$). $\kappa_{a,0}$ ($\kappa_{m,0}$) is the intrinsic loss of the optical (magnon) mode. $\Delta_1 = \omega_L - \omega_a$ and $\Delta_2 = \omega_{\mathrm{mw}} - \omega_m$ are the detuning of the optical pump and microwave, respectively. Through Eqs. (C4) and (C5), we have made numerical simulations, and all parameters are shown in Table 1.

The numerical results based on the parameter values above are shown in Fig. 3(b), which further validates our experimental results.

APPENDIX D

In our experiment, we used a Fabry–Perót (FP) cavity with an FSR of 10 GHz to estimate the conversion efficiency of the system. As shown in Fig. 2(a) in the main text, we measured the laser power after the prism, and simultaneously recorded the signal intensity measured by the FP cavity in the position of the PD. Then, we can get the corresponding relationship between the laser intensity emitted after the prism and the signal recorded by the oscilloscope. This method allows us to ignore the optical loss behind the prism in the optical path and directly obtain the intensity of the laser light emitted from the prism through an oscilloscope. As shown in Fig. 8(a), when the YIG microsphere is pumped by the microwave, the weak signal can be measured around the sideband of the pump laser through FP cavity. By recording the intensity of the sideband signal and the corresponding relationship between the laser intensity and the signal intensity obtained by the previous measurement, the output sideband signal from the prism can be calibrated. In our experiment, we measured the converted optical signal change with microwave power, as shown in Fig. 8(b). The slope of the fitted curve is the power conversion efficiency, and we determine the power conversion efficiency as about 3.62×10^{-6}. Taking the optical frequency (193 THz) and the magnon frequency (5 GHz) into consideration, the photon number conversion efficiency without insertion losses in our experiment is about 0.94×10^{-10}.

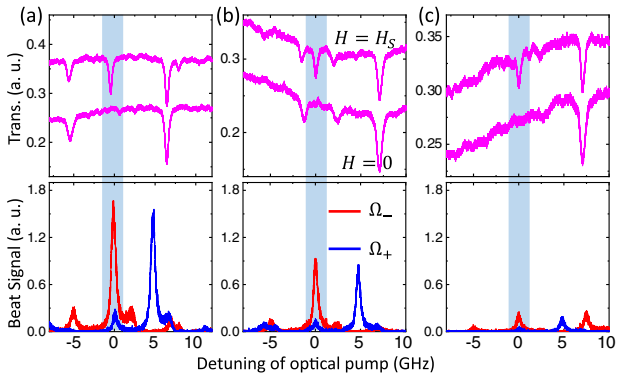

Fig. 7. (a)–(c) Transmission and the generated optical signal as a function of the optical pump laser detuning at various optical modes in one optical FSR. The target optical modes show the great change of transmission when the magnetic field intensity is zero (the bottom line) and H_S (the top line), and the SSB phenomenon will arise at these target optical modes (in the blue area).

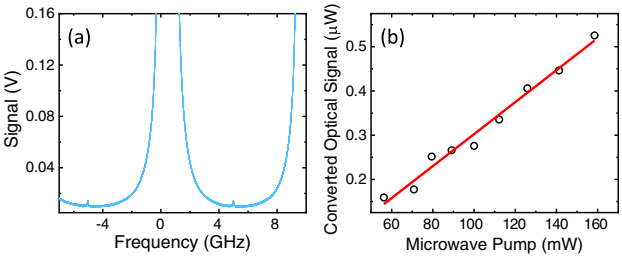

Fig. 8. (a) Sideband signal measured in a Fabry–Perót cavity. (b) Converted optical signal change with microwave power.

Funding. National Key Research and Development Program of China (2020YFB2205801); National Natural Science Foundation of China (11874342, 11934012, 61805229, 92050109); Fundamental Research Funds for the Central Universities; USTC Research Funds of the Double First-Class Initiative (YD2470002002).

Acknowledgment. C.-H. Dong was also supported by the State Key Laboratory of Advanced Optical Communication Systems and Networks, Shanghai Jiao Tong University, China. This work was partially carried out at the USTC Center for Micro and Nanoscale Research and Fabrication.

Disclosures. The authors declare no conflicts of interest.

Data Availability. Data underlying the results presented in this paper are not publicly available at this time but may be obtained from the authors upon reasonable request.

†These authors contributed equally to this work.

REFERENCES

1. R. W. Andrews, R. W. Peterson, T. P. Purdy, K. Cicak, R. W. Simmonds, C. A. Regal, and K. W. Lehnert, "Bidirectional and efficient conversion between microwave and optical light," Nat. Phys. **10**, 321–326 (2014).
2. J. Bochmann, A. Vainsencher, D. D. Awschalom, and A. N. Cleland, "Nanomechanical coupling between microwave and optical photons," Nat. Phys. **9**, 712–716 (2013).
3. A. Rueda, F. Sedlmeir, M. C. Collodo, U. Vogl, B. Stiller, G. Schunk, D. V. Strekalov, C. Marquardt, J. M. Fink, O. Painter, G. Leuchs, and H. G. L. Schwefel, "Efficient microwave to optical photon conversion: an electro-optical realization," Optica **3**, 597–604 (2016).
4. N. J. Lambert, A. Rueda, F. Sedlmeir, and H. G. Schwefel, "Coherent conversion between microwave and optical photons: an overview of physical implementations," Adv. Quantum Technol. **3**, 1900077 (2020).
5. L. Fan, C.-L. Zou, R. Cheng, X. Guo, X. Han, Z. Gong, S. Wang, and H. X. Tang, "Superconducting cavity electro-optics: a platform for coherent photon conversion between superconducting and photonic circuits," Sci. Adv. **4**, eaar4994 (2018).
6. X. Han, W. Fu, C.-L. Zou, L. Jiang, and H. X. Tang, "Microwave-optical quantum frequency conversion," Optica **8**, 1050–1064 (2021).
7. S. Barzanjeh, S. Guha, C. Weedbrook, D. Vitali, J. H. Shapiro, and S. Pirandola, "Microwave quantum illumination," Phys. Rev. Lett. **114**, 080503 (2015).
8. A. Vainsencher, K. Satzinger, G. Peairs, and A. Cleland, "Bi-directional conversion between microwave and optical frequencies in a piezoelectric optomechanical device," Appl. Phys. Lett. **109**, 033107 (2016).
9. K. C. Balram, M. I. Davanço, J. D. Song, and K. Srinivasan, "Coherent coupling between radiofrequency, optical and acoustic waves in piezo-optomechanical circuits," Nat. Photonics **10**, 346–352 (2016).
10. M. Soltani, M. Zhang, C. Ryan, G. J. Ribeill, C. Wang, and M. Loncar, "Efficient quantum microwave-to-optical conversion using electro-optic nanophotonic coupled resonators," Phys. Rev. A **96**, 043808 (2017).
11. A. P. Higginbotham, P. Burns, M. Urmey, R. Peterson, N. Kampel, B. Brubaker, G. Smith, K. Lehnert, and C. Regal, "Harnessing electro-optic correlations in an efficient mechanical converter," Nat. Phys. **14**, 1038–1042 (2018).
12. Y. Xu, A. A. Sayem, L. Fan, C.-L. Zou, S. Wang, R. Cheng, W. Fu, L. Yang, M. Xu, and H. X. Tang, "Bidirectional interconversion of microwave and light with thin-film lithium niobate," Nat. Commun. **12**, 4453 (2021).
13. T. Vogt, C. Gross, J. Han, S. B. Pal, M. Lam, M. Kiffner, and W. Li, "Efficient microwave-to-optical conversion using Rydberg atoms," Phys. Rev. A **99**, 023832 (2019).
14. B. T. Gard, K. Jacobs, R. McDermott, and M. Saffman, "Microwave-to-optical frequency conversion using a cesium atom coupled to a superconducting resonator," Phys. Rev. A **96**, 013833 (2017).
15. D. Petrosyan, K. Mølmer, J. Fortágh, and M. Saffman, "Microwave to optical conversion with atoms on a superconducting chip," New J. Phys. **21**, 073033 (2019).
16. S. Welinski, P. J. Woodburn, N. Lauk, R. L. Cone, C. Simon, P. Goldner, and C. W. Thiel, "Electron spin coherence in optically excited states of rare-earth ions for microwave to optical quantum transducers," Phys. Rev. Lett. **122**, 247401 (2019).
17. J. R. Everts, M. C. Berrington, R. L. Ahlefeldt, and J. J. Longdell, "Microwave to optical photon conversion via fully concentrated rare-earth-ion crystals," Phys. Rev. A **99**, 063830 (2019).
18. A. V. Chumak, V. I. Vasyuchka, A. A. Serga, and B. Hillebrands, "Magnon spintronics," Nat. Phys. **11**, 453–461 (2015).
19. M. Harder, Y. Yang, B. Yao, C. Yu, J. Rao, Y. Gui, R. Stamps, and C.-M. Hu, "Level attraction due to dissipative magnon-photon coupling," Phys. Rev. Lett. **121**, 137203 (2018).
20. Y. Tabuchi, S. Ishino, A. Noguchi, T. Ishikawa, R. Yamazaki, K. Usami, and Y. Nakamura, "Coherent coupling between a ferromagnetic magnon and a superconducting qubit," Science **349**, 405–408 (2015).
21. D. Lachance-Quirion, S. P. Wolski, Y. Tabuchi, S. Kono, K. Usami, and Y. Nakamura, "Entanglement-based single-shot detection of a single magnon with a superconducting qubit," Science **367**, 425–428 (2020).
22. D. Lachance-Quirion, Y. Tabuchi, A. Gloppe, K. Usami, and Y. Nakamura, "Hybrid quantum systems based on magnonics," Appl. Phys. Express **12**, 070101 (2019).
23. S. Viola Kusminskiy, H. X. Tang, and F. Marquardt, "Coupled spin-light dynamics in cavity optomagnonics," Phys. Rev. A **94**, 033821 (2016).
24. J. Graf, H. Pfeifer, F. Marquardt, and S. V. Kusminskiy, "Cavity optomagnonics with magnetic textures: coupling a magnetic vortex to light," Phys. Rev. B **98**, 241406 (2018).
25. Z.-X. Liu, B. Wang, H. Xiong, and Y. Wu, "Magnon-induced high-order sideband generation," Opt. Lett. **43**, 3698–3701 (2018).
26. X. Zhang, N. Zhu, C.-L. Zou, and H. X. Tang, "Optomagnonic whispering gallery microresonators," Phys. Rev. Lett. **117**, 123605 (2016).
27. A. Osada, R. Hisatomi, A. Noguchi, Y. Tabuchi, R. Yamazaki, K. Usami, M. Sadgrove, R. Yalla, M. Nomura, and Y. Nakamura, "Cavity optomagnonics with spin-orbit coupled photons," Phys. Rev. Lett. **116**, 223601 (2016).
28. A. Osada, A. Gloppe, R. Hisatomi, A. Noguchi, R. Yamazaki, M. Nomura, Y. Nakamura, and K. Usami, "Brillouin light scattering by magnetic quasivortices in cavity optomagnonics," Phys. Rev. Lett. **120**, 133602 (2018).
29. J. A. Haigh, A. Nunnenkamp, A. J. Ramsay, and A. J. Ferguson, "Triple-resonant Brillouin light scattering in magneto-optical cavities," Phys. Rev. Lett. **117**, 133602 (2016).
30. N. Zhu, X. Zhang, X. Han, C.-L. Zou, C. Zhong, C.-H. Wang, L. Jiang, and H. X. Tang, "Waveguide cavity optomagnonics for broadband multimode microwave-to-optics conversion," Optica **7**, 1291–1297 (2020).
31. R. Hisatomi, A. Noguchi, R. Yamazaki, Y. Nakata, A. Gloppe, Y. Nakamura, and K. Usami, "Helicity-changing Brillouin light scattering by magnons in a ferromagnetic crystal," Phys. Rev. Lett. **123**, 207401 (2019).
32. C.-H. Dong, Z. Shen, C.-L. Zou, Y.-L. Zhang, W. Fu, and G.-C. Guo, "Brillouin-scattering-induced transparency and non-reciprocal light storage," Nat. Commun. **6**, 6193 (2015).
33. M. Aspelmeyer, T. J. Kippenberg, and F. Marquardt, "Cavity optomechanics," Rev. Mod. Phys. **86**, 1391–1452 (2014).
34. C.-Z. Chai, H.-Q. Zhao, H. X. Tang, G.-C. Guo, C.-L. Zou, and C.-H. Dong, "Non-reciprocity in high-Q ferromagnetic microspheres via photonic spin–orbit coupling," Laser Photon. Rev. **14**, 1900252 (2020).
35. K. Y. Bliokh, F. J. Rodríguez-Fortuño, F. Nori, and A. V. Zayats, "Spin–orbit interactions of light," Nat. Photonics **9**, 796–808 (2015).
36. K. Y. Bliokh, D. Smirnova, and F. Nori, "Quantum spin Hall effect of light," Science **348**, 1448–1451 (2015).
37. Z. Shen, Y.-L. Zhang, Y. Chen, C.-L. Zou, Y.-F. Xiao, X.-B. Zou, F.-W. Sun, G.-C. Guo, and C.-H. Dong, "Experimental realization of optomechanically induced non-reciprocity," Nat. Photonics **10**, 657–661 (2016).
38. T. J. Kippenberg and K. J. Vahala, "Cavity optomechanics: back-action at the mesoscale," Science **321**, 1172–1176 (2008).
39. E. E. Wollman, C. U. Lei, A. J. Weinstein, J. Suh, A. Kronwald, F. Marquardt, A. A. Clerk, and K. C. Schwab, "Quantum squeezing of motion in a mechanical resonator," Science **349**, 952–955 (2015).
40. U.-S. Lee, H.-D. Jung, and S.-K. Han, "Optical single sideband signal generation using phase modulation of semiconductor optical amplifier," IEEE Photon. Technol. Lett. **16**, 1373–1375 (2004).

41. C.-Z. Chai, X.-X. Hu, C.-L. Zou, G.-C. Guo, and C.-H. Dong, "Thermal bistability of magnon in yttrium iron garnet microspheres," Appl. Phys. Lett. **114**, 021101 (2019).
42. N. J. Lambert, J. A. Haigh, and A. J. Ferguson, "Identification of spin wave modes in yttrium iron garnet strongly coupled to a co-axial cavity," J. Appl. Phys. **117**, 053910 (2015).
43. J. A. Haigh, N. J. Lambert, S. Sharma, Y. M. Blanter, G. E. W. Bauer, and A. J. Ramsay, "Selection rules for cavity-enhanced Brillouin light scattering from magnetostatic modes," Phys. Rev. B **97**, 214423 (2018).
44. C.-L. Zou, X.-B. Zou, F.-W. Sun, Z.-F. Han, and G.-C. Guo, "Room-temperature steady-state optomechanical entanglement on a chip," Phys. Rev. A **84**, 032317 (2011).